Eigenvector alignment: assessing functional network changes in amnestic mild cognitive impairment and Alzheimer's disease

Ruaridh Clark[1*], Niia Nikolova[2], William J. McGeown[2], Malcolm Macdonald[1]

1 Mechanical and Aerospace Engineering, University of Strathclyde, Glasgow, UK
2 School of Psychological Sciences and Health, University of Strathclyde, Glasgow, UK

* ruaridh.clark@strath.ac.uk

Abstract

This paper adapts a method for detecting influential nodes and communities in networked systems to reveal changes in functional networks of subjects with Alzheimer's disease (AD) and amnestic Mild Cognitive Impairment (aMCI). Well-established methods exist for analysing connectivity networks composed of brain regions, including the widespread use of centrality metrics such as eigenvector centrality. However, these metrics provide only limited information on the relationship between regions, with this understanding often sought by comparing the strength of pairwise functional connectivity. Our holistic approach, eigenvector alignment, considers the impact of all the functional connectivity changes on the alignment of any two regions. This is achieved by comparing their placement in a Euclidean space defined by the network's dominant eigenvectors. Eigenvector alignment reveals that key regions in the Default Mode Network lack clear and consistent alignments in healthy control subjects. This results in relatively few significant alignment changes in AD, despite clear reductions in functional connectivity within this network. For AD subjects, compared with healthy controls, the posterior superior temporal gyrus displays the most significant bilateral decrease in alignment where both sides become significantly more aligned with the brainstem. Substantial realignments were also noted bilaterally within regions such as the Heschl's gyrus and the planum polare, which begin in aMCI, and result in these brain regions having significantly increased separation from each other in AD. These findings present a case for the use of eigenvector alignment, alongside established network analytic approaches, to capture how the brain's functional networks develop and adapt when challenged by disease processes such as AD.

Introduction

Functional connectivity is one of the gateways through which a network representation of the brain's interactions can be sought. These connectivities can be weighted based on the strength of the correlations between regions over time. The measures may provide information on the underlying reasons that clinical symptoms occur at different disease stages. Researchers have used functional connectivity values to assess changes in the strength of interaction between groups of key regions [1, 2]. These methods can provide clear results but do not take the holistic view required to capture how variations in functional connectivity can change the functional networks of the brain. Graph theory and network neuroscience methods exist for evaluating structural network changes [3],

with the assessment of functional connectivity of subjects in resting-state a popular field of study [4]. But these graph structural assessments do not explicitly capture the changing relationship between nodes. It is also important to note that these methods often require binarisation and thresholding of the functional connectivity matrices, which are all-to-all, weighted, adjacency matrices. Binarisation produces an unweighted graph, which is potentially an inaccurate representation of a neuronal network since connections are known to vary in strength [5]. Thresholds are frequently applied to remove potentially spurious low weight connections, but their application can be controversial as the choice of threshold value can affect the results [5–7]. To address this problem some unbiased thresholds have been proposed, such as the Cluster-Span Threshold in [8].

This paper focuses on Alzheimer's disease (AD) and amnestic Mild Cognitive Impairment (aMCI). AD is the most common type of dementia. It is typically characterised by a marked decline in episodic memory, with deficits occurring in other cognitive domains such as in language, visuospatial and executive functioning. Individuals with aMCI present with impairments in memory, but their other cognitive domains remain relatively intact. Not all individuals with aMCI are in the early stages of AD, but people with this pattern of symptomology are at high risk of conversion to the disorder [9]. There has been a large body of work documenting the changes in regional brain volume as AD progresses, for example, individuals with aMCI that later convert to Alzheimer's disease have been shown to have greater atrophy of the left hippocampus than those who do not [10]. Volumetric analysis is useful but it does not inform on how brain dynamics are modified by AD, with *functional magnetic resonance imaging* (fMRI), the data is able to offer information on the regulation of brain networks that can provide additional markers of disease. Decreased functional connectivity has also been proposed as biomarker for AD [11].

The theoretical basis for eigenvector alignment, proposed in this paper as a tool for detecting and quantifying changes in functional alignment, is a method of influential community detection, referred to as communities of dynamical influence (CDI) [12]. Communities are usually detected by an increased density of connections, but for CDI this density is implicitly captured by proximity and alignment to the network's most influential nodes. Communities have been detected in a similar manner before, with [13] also employing eigenvectors to define divisions in the network structure, and CDI itself has been applied in the same context of comparing AD and aMCI subjects [14]. But by breaking CDI down into its two main components, which are eigenvector centrality and eigenvector alignment, we can gain insights into the shifting relationships between brain regions. Eigenvector centrality is an established metric in network science for determining the influence of a network node in terms of the flow of information around a system [15, 16]. Eigenvector alignment is presented herein as a method to determine the alignment of Regions of Interest (ROIs) when they are embedded in Euclidean space defined by the system's dominant eigenvectors. Eigenvectors capture every change in functional connectivity to provide an insight into functional network changes across the whole brain, with eigenvector alignment able to identify the impact on any two ROIs. Interestingly, our approach draws strong parallels to [17, 18], where a measure of functional connectivity itself is derived by converting ROIs from an anatomical space to a functional space (or eigenimage).

Eigenvectors have been used previously to identify circuitry in neuronal networks, where [19] essentially applied spectral bisection but using a selection of eigenvectors, not just the second dominant eigenvector, to reveal known associations of neurons in a *C. elegans* neuronal network. An expansion of this approach for identifying neuronal circuitry, but using multiple eigenvectors in combination, has also been presented in [20].

Eigenvector alignment is applied throughout this paper using three dominant

eigenvectors, which is suggested in [12] as a trade-off between capturing community structure from the network and ensuring that those communities represent the most important divisions in terms of information flow dynamics. The most dominant eigenvectors are associated with the eigenvalues of largest magnitude. When treating the adjacency matrix as a linear transformation these eigenvectors capture the direction of greatest linear change for this transformation. Hence, these vectors highlight the ROIs that are most important for the movement of information around the network and likely to be the most critical if disrupted.

Materials and methods

In order to compare the functional connectivity between the AD, aMCI and Healthy Control (HC) groups, a connectivity matrix is generated for each subject from their resting-state fMRI scan. The connectivity is only considered between a series of predefined brain regions, each defined as a ROI. This results in an all-to-all, weighted and undirected connectivity matrix that captures the strength of the functional connectivity between ROIs. A threshold is applied to reduce the weakest connections and the dominant eigenvectors are calculated for each matrix. These eigenvectors then form the basis for comparing subjects within and between the AD, aMCI and HC groups.

Dataset

The fMRI resting state data that is analysed in this work is from the 'Resting-state fMRI in Dementia Patients' dataset [21] (Harvard Dataverse). The MRI data was obtained using a Siemens 3T MRI system (Magnetom Allegra, Siemens, Erlangen, Germany) for ten patients with a probable AD diagnosis (by NINCDS-ADRDA consensus criteria [22]), 10 aMCI patients [23] and 10 healthy elderly subjects (HC).

The subjects underwent a resting state echo-planar imaging (EPI) fMRI scan (TR = 2080 ms, TE = 30 ms, 32 axial slices parallel to AC-PC plane, matrix 64×64, in plane resolution $3 \times 3\,\mathrm{mm}^2$, slice thickness = 2.5 mm, 50% skip, flip angle = 70 degrees). The duration of the scan was 7 minutes and 20 seconds, yielding 220 volumes. Subjects were instructed to keep their eyes closed throughout, refrain from thinking of anything in particular and to avoid falling asleep. An anatomical T1-weighted three dimensional MDEFT (modified driven equilibrium Fourier transform) scan was also acquired for each subject (TR = 1338 ms, TE = 2.4 ms, TI = 910 ms, flip angle = 15 degrees, matrix = $256 \times 224 \times 176$, FOV = $256 \times 224\,\mathrm{mm}^2$, slice thickness = 1 mm, total scan time = 12 min).

Preprocessing

The functional data is preprocessed using the CONN toolbox (CONN: functional connectivity toolbox, [24]) for SPM12 (`www.fil.ion.ucl.ac.uk/spm`) and MATLAB version 2018a.

Spatial Preprocessing

The first four volumes of the functional scans were removed in order to eliminate any saturation effects and to allow the signal to stabilise. Functional data is slice-time adjusted and corrected for motion. The high resolution T1 weighted anatomical images were coregistered with the mean EPI image. They were segmented into grey matter (GM), white matter (WM), and cerebrospinal fluid (CSF) masks and were spatially

normalised to the Montreal Neurological Institute (MNI) space [25]. The obtained transformation parameters were then applied to the motion corrected functional data, and an 8mm FWHM Gaussian kernel was applied for spatial smoothing. It should be noted that the use of spatial smoothing on fMRI data can affect the properties of functional brain networks, including a possible over-emphasis on strong, short-range, links as well as changes in the identities of hubs of the network and decreased inter-subject variation [26].

Temporal Filtering

The aCompCor technique is applied to mitigate against physiological and movement-related noise. This technique identifies and removes the first five principal components of the signal from the CSF and WM masks (eigenvectors of the PCA decomposition of the EPI timecourse averaged over the CSF and WM), as well as the motion parameters, their first-order temporal derivatives and a linear detrending term [27]. This process resulted in the exclusion of one subject from the AD group due to excessive motion. Scrubbing and motion regression were also performed with the preprocessed functional data then it was bandpass filtered ($0.008\text{Hz} < f < 0.09\text{Hz}$) using a fast Fourier transform (FFT).

Connectivity Matrix Generation

The CONN atlas, which combines the FSL Harvard-Oxford cortical and subcortical areas and the AAL atlas cerebellar areas, is used to define one hundred and thirty-two (132) ROIs. Connectivity between the 132 ROIs is assessed for each subject using their 7-minute resting state scan. We constructed 132 x 132 ROI-to-ROI correlation (RRC) matrices of Fisher z-transformed bivariate correlation coefficients (Pearson's r) using the ROIs described above. For each subject, a graph adjacency matrix $A(i, j)$ is computed by thresholding the RRC matrix r(i,j) using the Cluster-Span Threshold (CST [8]).

Cluster-Span Threshold

An unbiased Cluster-Span Threshold (CST) [8] is used for generating the adjacency matrix. CST is especially suitable as it is able to distinguish between HC and AD subjects when applied to their functional connectivity matrices [28]. The threshold is defined based on a clustering coefficient, C, that for a given network balances the number of triples that are clustered, forming loops, with those that are spanning, forming trees. A triple is formed by at least two edges connecting 3 nodes. Triples that are also clustered are those that form triangles where each of the three nodes are connected to the other two. A triple that does not form a triangle/cluster is defined as a spanning triple. The threshold generates a topology that excludes edges with weights smaller than the chosen value. CST is selected so that the topology generated contains the same number of clustered triples and spanning triples. The use of thresholds is a common practice to filter out connections that may only be present because of noise in the fMRI data. The choice of threshold can affect the results of a study [5–7], so we briefly compare the use of CST in the Results section with a selection of arbitrary thresholds.

Communities of Dynamical Influence

For each subject's connectivity network, the ROIs can be assigned into communities of dynamical influence (CDI) based on the strength and selection of their connections. CDI identifies communities based on their alignment in Euclidean space defined by multiple

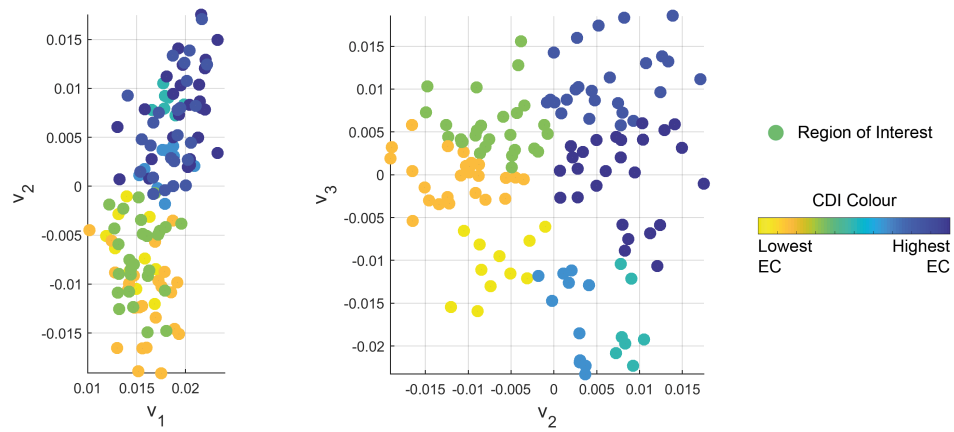

Fig 1. An AD subject's ROIs embedded in an eigenvector space where v_1,v_2, and v_3 are the three most dominant eigenvectors of the adjacency matrix. Each community of dynamical influence (CDI) is coloured based on their largest eigenvector centrality (EC) value.

(often three) of the system's dominant eigenvectors (those associated with the dominant eigenvalues). The nodes, which are further from the origin of this coordinate system than any of their connections, are defined as leaders of separate communities. Each of these communities is populated with other nodes that lie on a path that connects to the leader node of that community. Each node is assigned to only one community, where the community is chosen by assessing which leader is in closest alignment to that node. This alignment is assessed by comparing the position vector, from the origin of the coordinate system, for the leader nodes with the node to be assigned. The dot product of these position vectors determines the leader that is aligned most closely to that node. The application of CDI on an AD subject's adjacency matrix of functional connectivity is shown in Figure 1, where the network is divided into seven communities.

Once community designation is complete, the order of influence is determined by evaluating the largest entry of the most dominant eigenvector for each community (i.e. eigenvector centrality (EC) [15, 16]) that is known to be a non-negative vector. The community that contains the node with the largest EC value ($\mathbf{v}_1$) is ranked as the most influential community, with the other communities ranked in descending order according to their largest EC value.

In this paper, CDI is determined from the three most dominant eigenvectors of the undirected connectivity matrix after applying CST. These are the eigenvectors associated with the largest eigenvalues in magnitude and are shown in [12] to identify the nodes that are most effective at driving a directed network to consensus.

Eigenvector Alignment

The alignment between every ROI with respect to every other ROI can be identified by embedding the ROIs in a vector space, defined by the system's three dominant eigenvectors, and assessing the dot product of their position vectors, with respect to the origin of this coordinate frame. This comparison can yield the angle, referred to throughout as alignment, between the two vectors using the well-known relation,

$$\theta = \cos^{-1}\left(\frac{\mathbf{r}\cdot\mathbf{s}}{|\mathbf{r}||\mathbf{s}|}\right) \tag{1}$$

where **r** and **s** are the position vectors for different ROIs in the eigenvector based coordinate frame. ROIs are highly aligned when they have a small angle between their position vectors. The significance of these differences in alignment are determined when $p < 0.05$ using a two-sample t test for comparing between the HC, aMCI and AD groups.

Results

In [28] clustering coefficient and degree variance were used to demonstrate that Cluster-Span Threshold (CST) is a sensitive threshold for AD detection. In this paper, the CST value is applied to the functional connectivity networks of 29 subjects with values varying between 0.24 and 0.27.

We demonstrate the effectiveness of CST by first dividing the network into communities of dynamical influence (CDI), which are ranked based on their eigenvector centrality as described in the Communities of Dynamical Influence section. This enables the most and least influential communities to be identified. When using CST, the number of ROIs in the most and the least influential community are seen to significantly vary ($p = 0.027$ and $p = 0.004$ respectively) for the AD subjects compared with the HC group. The difference in community size is not significant for either the most or least influential CDI in the other comparisons, namely AD versus aMCI ($p = 0.098$ and $p = 0.180$, respectively) and aMCI versus HC ($p = 0.774$ and $p = 0.229$, respectively).

It is known that the choice of threshold can influence the result of network analysis. We explored the impact of varying the threshold on the community size comparisons. When performing the same comparison using a range of constant threshold values between 0 and 0.9, at 0.1 increments, it is not possible to replicate the significance, seen with CST, for both the most and least influential CDI in the AD versus HC comparison. For some of the other threshold values two of the six results were significant, which were always a combination of one significant result from the AD versus HC case and one from the AD versus aMCI case. For the lower constant thresholds, below 0.4, significance is only achieved when comparing the size of the least influential community. For the threshold at 0.5, significance is seen for the most influential in AD versus HC

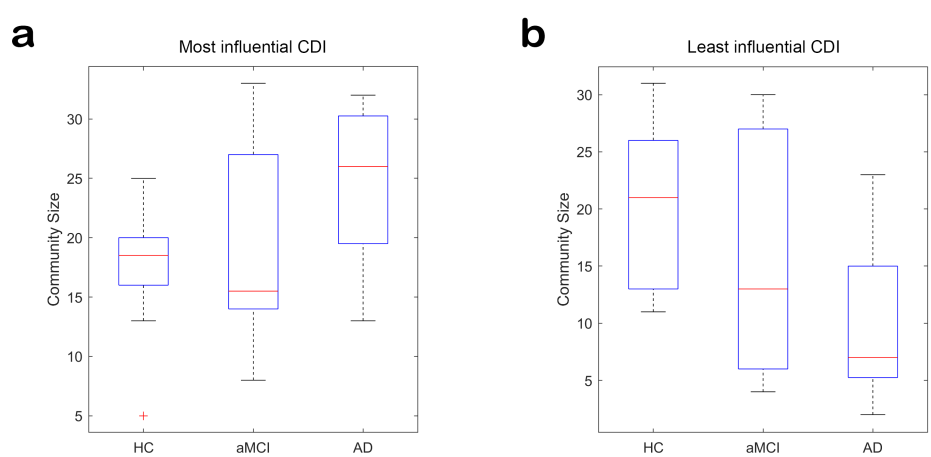

Fig 2. The variation in community size of (a) the most influential CDI and (b) the least influential CDI for subjects in the HC, aMCI and AD groups. The median, 25th and 75th percentile are detailed with the whiskers extending to the most extreme data points. Outliers lie more than three scaled median absolute deviations away from the median and are excluded.

and least influential in AD vs aMCI. For the higher threshold at 0.7 only the most influential community differences were significant. The CST appears to find a balance between these high and low thresholds by showing significant differences in the size of both the most and least influential communities.

The CST's ability to differentiate between AD and HC subjects [28] appears to reinforce the case for using three eigenvectors for the communities of dynamical influence [12] and, hence, eigenvector alignment in this work. As CDI generated from two, four, or five dominant eigenvectors failed to significantly differentiate between any of the groups when applying CST (lowest p value in AD versus HC comparison is $p = 0.274$ for the four eigenvector CDI). This comparison is based on community size, as before. Only the four eigenvector CDI differentiates between AD and HC groups with any of the tested threshold values. This difference is seen for the least influential CDI when no weighting is applied ($p = 0.033$).

Visualising alignment

Two of the most significant eigenvector alignment changes, from the AD-HC comparison, are highlighted in Figure 3 by displaying the ROIs in a Euclidean plane defined by the 2nd and 3rd dominant eigenvectors (v_2 and v_3) of the adjacency matrix. The most significant decrease in alignment in the AD group is between the left and the right division of the pSTG ($p = 7 \times 10^{-4}$), shown in Figure 3 **a** and **c**. This is displayed alongside another significant increase in alignment for the AD group between the right division of the posterior superior temporal gyrus (pSTG) and the brainstem ($p = 2 \times 10^{-5}$), shown in Figure 3 **b** and **d**.

Figure 3 **a** details the close alignment of the left and right divisions of the pSTG, in HC subjects, with a mean alignment angle $\bar{\theta} = 0.29$ radians. This is in contrast to Figure 3 **c** of the same two ROIs, in AD subjects, where the mean angle increases to $\bar{\theta} = 0.92$ rad.

The right pSTG is poorly aligned with the brainstem, for HC subjects, with a mean $\bar{\theta} = 1.60$ rad. This lack of alignment is visually clear, in Figure 3 **b**, with the line between the ROIs crossing at least one axis and, for half of the subjects, crossing both axes. Again there is a contrast with the AD group where the mean angle decreases to $\bar{\theta} = 0.68$ rad for this alignment. This closer alignment can be seen in Figure 3 **d** where there are only a few lines crossing axes and one of those belongs to a pair of closely aligned ROIs near the origin.

Interestingly, the left pSTG also becomes significantly more aligned with the brainstem ($p = 9 \times 10^{-4}$), for the AD-HC comparison, despite having a decreased alignment with the right pSTG. This shift is highly significant bilaterally due to the lack of alignment in HC subjects between the pSTG and brainstem. The mean alignment angle, with respect to the brainstem, is $\bar{\theta} = 1.614$ rad for the left and $\bar{\theta} = 1.603$ rad for the right pSTG in the HC group. This becomes $\bar{\theta} = 0.888$ rad for the left and $\bar{\theta} = 0.682$ rad for the right in the AD group.

The brainstem is among one of the most aligned ROIs for the right pSTG in the AD group. The only more aligned ROIs, for the right pSTG, are the left cuneus ($\bar{\theta} = 0.649$ rad) and the left supracalcarine cortex ($\bar{\theta} = 0.680$ rad). Whereas the brainstem is less notably aligned to the left pSTG, which is most closely aligned to the left temporo-occipital middle temporal gyrus ($\bar{\theta} = 0.682$ rad) and the left superior frontal gyrus ($\bar{\theta} = 0.763$ rad).

The increased separation of the left and right divisions of pSTG has been highlighted before in [29] where AD is noted to cause disruption of the commissural system connecting the bilateral temporal and parietal cortical areas. Given the reported commissural system disruption in parietal cortical areas [29], it is notable that a significantly reduced alignment is also seen between the left and right superior parietal

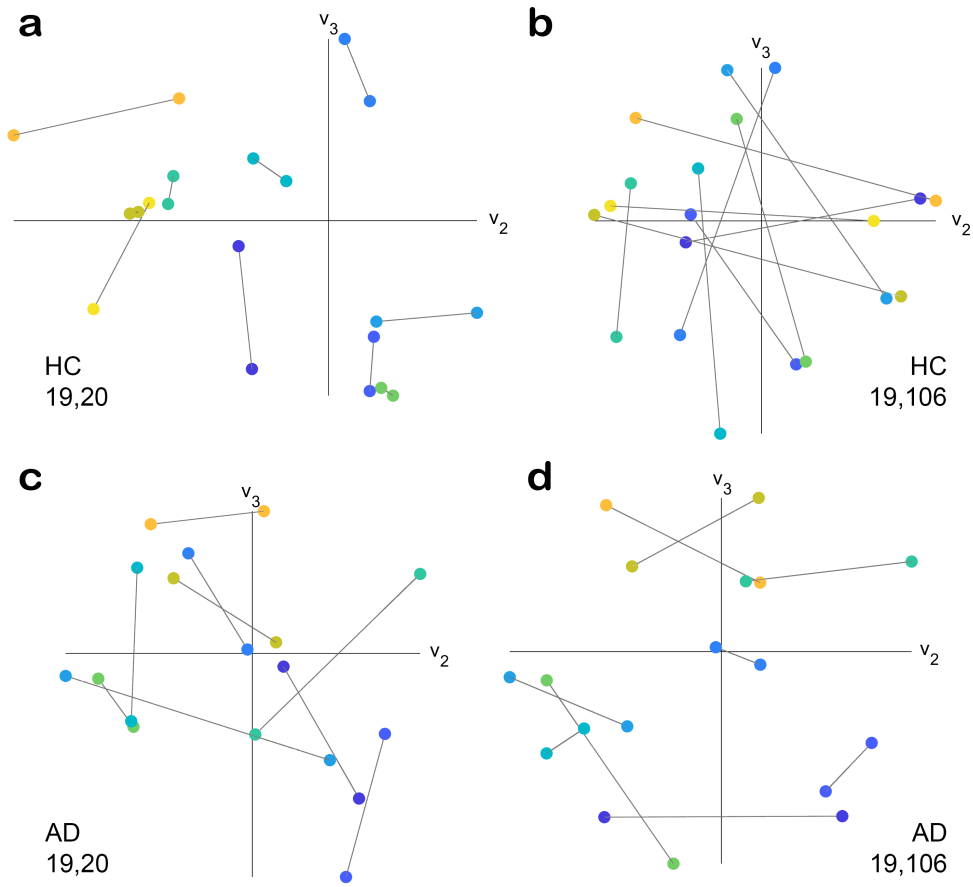

Fig 3. Comparison between the right (19) and left (20) division of the posterior superior temporal gyrus (pSTG) in **a** and **c** alongside a comparison between the right division of the pSTG (19) and the brainstem (106) in **b** and **d**. A line connects the two regions in each plot if they belong to the same subject. The HC subjects are shown in **a** and **b** and the AD subjects in **c** and **d**.

lobules (SPL) in the AD versus HC comparison ($p = 0.026$). In AD subjects, the left SPL is most aligned with the left juxtapositional lobule ($\bar{\theta} = 0.575$ rad) and the left precentral gyrus ($\bar{\theta} = 0.655$ rad). While the right SPL is most aligned with the left anterior supramarginal gyrus ($\bar{\theta} = 0.603$ rad) and the frontal medial cortex ($\bar{\theta} = 0.678$ rad).

The aMCI group also displays significant changes for the right pSTG, versus the HC group, with a significant decrease in alignment with respect to the left pSTG ($p = 0.039$) and an increase in alignment with respect to the brainstem ($p = 0.036$). In both cases aMCI is at an intermediary stage between what is observed from the HC and AD group. The left pSTG does not display a significant change with respect to the brainstem in the aMCI-HC comparison. The only significant change in alignment for the AD-aMCI comparison is with the right pSTG and the brainstem ($p = 0.023$).

Alzheimer's Disease

Table 1 details the ROIs with the largest number of significant changes in alignment between the AD and HC groups. This number does not distinguish between an increase

or decrease in alignment, as both are present for those listed in Table 1. The left Heschl's gyrus and the bilateral planum polare are prominent in Table 1, where it is notable that these two ROIs are in close alignment for HC subjects but become significantly less aligned in the AD group. Both sides of the Heschl's gyrus have a significant reduction in alignment with respect to the planum polare, but there is a greater change in mean alignment for the left Heschl's gyrus when compared with the left ($\Delta\bar{\theta} = 0.97$ rad, $p = 0.008$) and right planum polare ($\Delta\bar{\theta} = 0.91$ rad, $p = 0.007$).

The most aligned ROI pair among the AD subjects are the left central opercular cortex and the left parietal operculum ($\bar{\theta} = 0.24$ rad). While the least aligned ROI pair are the right occipital fusiform gyrus and left frontal orbital cortex ($\bar{\theta} = 2.33$ rad). In the AD-HC comparison, the biggest decrease in alignment is between the subcallosal cortex and vermis 4 & 5 ($\Delta\bar{\theta} = 1.22$ rad, $p = 6 \times 10^{-4}$). The biggest increase in alignment is between the right pSTG) and the brainstem ($\Delta\bar{\theta} = 1.24$ rad, $p = 2 \times 10^{-5}$).

The ROIs in Table 1 are not the same as those that show the most significant changes in eigenvector centrality (EC). For the AD-HC group comparison, a significant decrease in EC is observed for the right posterior middle temporal gyrus ($p = 0.027$), left superior parietal lobule ($p = 0.049$), left juxtapositional lobule ($p = 0.044$) and anterior cingulate gyrus ($p = 0.016$). Alongside an increase in EC for the right caudate ($p = 0.012$), left cerebellum 4 & 5 ($p = 0.030$), and vermis 10 ($p = 0.001$).

ID	ROI	AD-HC
85	Heschl's gyrus Left	26
82	Planum Polare Right	22
63	Parahippocampal gyrus, anterior Left	19
83	Planum Polare Left	18
4	Insular cortex Left	17
44	Lateral Occipital cortex, superior Left	17
54	Paracingulate gyrus Left	17
68	Temporal Fusiform cortex, anterior Right	17
123	Cerebellum 10 Left	17
86	Planum Temporale Right	15

Table 1. For the AD comparison with HC (AD-HC), the ROIs with the largest number of significant eigenvector alignment changes ($p < 0.05$), with respect to other ROI, are detailed.

Amnestic Mild Cognitive Impairment

Table 2 displays the ROIs with the largest number of significant changes in alignment between the aMCI and HC groups. For a number of the entries in Table 2 – namely the left pallidum, bilateral nucleus accumbens, and left superior lateral occipital cortex – significant changes are consistently seen with respect to one or both sides of the bilateral central opercular cortex, parietal operculum cortex, planum polare, Heschl's gyrus, and planum temporale. These are interesting to note, especially given the prominent number of changes seen for the planum polare, Heschl's gyrus, and planum temporale in AD, see Table 1.

The most aligned ROI pair, among the aMCI subjects, are the left and right postcentral gyri ($\bar{\theta} = 0.27$ rad). While the least aligned ROIs are the left posterior temporal fusiform cortex and right Heschl's gyrus ($\bar{\theta} = 2.21$ rad). In the aMCI-HC comparison, the biggest decrease in alignment is between the right juxtapositional lobule and left pallidum ($\Delta\bar{\theta} = 1.34$ rad, $p = 1 \times 10^{-4}$). The biggest increase in

alignment is between the right anterior middle temporal gyrus and the right thalamus ($\Delta\bar{\theta} = 1.15$ rad, $p = 9 \times 10^{-4}$).

The right posterior middle temporal gyrus, reported in Table 2 for significant changes in eigenvector alignment, is noteworthy for also having a significant change in its eigenvector centrality (EC) between the aMCI and HC groups. Significant EC decreases are observed in right posterior middle temporal gyrus ($p = 0.024$), vermis 7 ($p = 0.043$) and vermis 10 ($p = 0.012$). Significant EC increases are observed in the right posterior ($p = 0.042$) and left temporooccipital inferior temporal gyrus ($p = 0.020$), right occipital fusiform gyrus ($p = 0.047$), and right cerebellum 8 ($p = 0.021$).

ID	ROI	MCI-HC
99	Pallidum Left	34
64	Parahippocampal gyrus, posterior Right	27
104	Accumbens Right	26
23	Middle Temporal gyrus, posterior Right	21
24	Middle Temporal gyrus, posterior Left	18
44	Lateral Occipital cortex, superior Left	18
105	Accumbens Left	18
110	Cerebellum Crus2 Right	18

Table 2. For the aMCI comparison with HC (aMCI-HC), the ROIs with the largest number of significant eigenvector alignment changes ($p < 0.05$), with respect to other ROI, are detailed.

aMCI compared to AD

Table 3 compares the AD and aMCI groups on the largest number of significant alignment changes, demonstrating that the inferior and middle temporal gyrus feature prominently. The biggest decrease in alignment from aMCI to AD is between the right frontal orbital cortex and right amygdala ($\Delta\bar{\theta} = 1.21$ rad, $p = 6 \times 10^{-4}$). The biggest increase in alignment from aMCI to AD is between the right posterior inferior temporal gyrus and the right Heschl's gyrus ($\Delta\bar{\theta} = 1.19$ rad, $p = 2 \times 10^{-5}$).

The left planum polare is placed prominently by both the eigenvector alignment and centrality (EC) metrics. Significant decreases in EC are seen for the anterior cingulate cortex ($p = 0.044$) and the left planum polare ($p = 0.043$), while a significant increase in EC is noted for the left anterior supramarginal gyrus ($p = 0.026$).

Hippocampal regions

The parahippocampal gyrus displays some notable changes in eigenvector alignment, which are captured in Table 4. In [30], the posterior parts of the parahippocampal gyri (pPHG) were found to be preferentially affected in age related memory decline. This is noted in [30] to contrast with AD, where the anterior of the parahippocampal gyri (aPHG) has been found to be more severely affected [31, 32]. This pathology is supported by the results in Table 4, which reports a high number of significant changes in eigenvector alignment for the left and right aPHG, in the AD-HC comparison (19 and 14 respectively). While the largest change for the left and right pPHG is seen in the aMCI-HC comparison (10 and 27 respectively). Table 4 also reveals that there are only a few significant changes in eigenvector alignment for the pPHG in the AD-HC case, despite the high variation in the aMCI-HC case.

For the hippocampus, Table 4 shows that the greatest change in alignment occurs between AD and aMCI subjects. For this comparison, AD subjects show significantly

ID	ROI	AD-MCI
30	Inferior Temporal gyrus, posterior Left	29
31	Inferior Temporal gyrus, temporooccipital part Right	28
24	Middle Temporal gyrus, posterior Left	27
110	Cerebellum Crus2 Right	26
29	Inferior Temporal gyrus, posterior Right	21
68	Temporal Fusiform cortex, anterior Right	21
101	Hippocampus Left	21
83	Planum Polare Left	19
70	Temporal Fusiform cortex, posterior Right	18
82	Planum Polare Right	18
91	Occipital Pole Left	17
1	Frontal Pole Right	16
5	Superior Frontal gyrus Right	16

Table 3. For the AD comparison with aMCI (AD-aMCI), the ROIs with the largest number of significant eigenvector alignment changes ($p < 0.05$), with respect to other ROI, are detailed.

ID	ROI	AD-HC	aMCI-HC	AD-aMCI
62	Parahippocampal gyrus, anterior Right	14	5	5
63	Parahippocampal gyrus, anterior Left	19	7	12
64	Parahippocampal gyrus, posterior Right	2	27	15
65	Parahippocampal gyrus, posterior Left	3	10	8
100	Hippocampus Right	4	3	10
101	Hippocampus Left	2	10	21

Table 4. Hippocampal regions: The number of significant changes in eigenvector alignment ($p < 0.05$) for each ROI with respect to other ROI are detailed for AD subjects compared to HC (AD-HC) as well as aMCI subjects compared to HC (aMCI-HC) and AD subjects compared to aMCI (AD-aMCI).

increased alignment for the hippocampus bilaterally with the right pPHG. The hippocampus shows a significant bilateral decrease in alignment to the left middle frontal, the left inferior frontal regions (pars triangularis and pars opercularis), the left superior parietal lobule, the left supramarginal gyrus (anterior and posterior divisions), and the left parietal operculum.

In the aMCI group the left hippocampus is in closest alignment (according to the mean alignment angle) with the left, pars triangularis, inferior frontal Gyrus and the right hippocampus is closest to the left temporal pole. These alignments significantly decrease in AD subjects, with the left hippocampus in closest alignment to the right hippocampus and the right hippocampus closest to the left amygdala.

Default Mode Network

It has been repeatedly observed that the Default Mode Network (DMN) is affected by AD and aMCI with the posterior cingulate gyrus and precuneus often the focus of such studies [33]. We find that ROIs in the DMN are repeatedly highlighted by eigenvector centrality (EC) in each of the comparisons in this paper; decreased EC for the anterior

cingulate in both the AD versus HC ($p = 0.016$) and AD versus aMCI ($p = 0.044$), decreased EC for the right angular gyrus in the aMCI versus HC comparison ($p = 0.024$) and increased EC for the left anterior supramarginal gyrus in AD versus aMCI ($p = 0.026$). In contrast, these regions do not show a large number of significant changes in eigenvector alignment, see Table 5. The main exception is the left paracingulate gyrus for both the AD group and aMCI group when compared with HC subjects.

ID	ROI	AD-HC	aMCI-HC	AD-aMCI
53	Paracingulate gyrus Right	9	8	4
54	Paracingulate gyrus Left	17	15	4
55	Cingulate gyrus, anterior	0	5	8
56	Cingulate gyrus, posterior	2	6	3
57	Precuneus cortex	2	5	6
37	Supramarginal gyrus, anterior Right	3	5	2
38	Supramarginal gyrus, anterior Left	3	5	6
39	Supramarginal gyrus, posterior Right	3	9	4
40	Supramarginal gyrus, posterior Left	4	4	9
41	Angular gyrus Right	7	4	4
42	Angular gyrus Left	2	6	6

Table 5. Default Mode Network and related ROI: The number of significant changes in eigenvector alignment ($p < 0.05$) for each ROI with respect to other ROI are detailed for AD subjects compared to HC (AD-HC) as well as aMCI subjects compared to HC (aMCI-HC) and AD subjects compared to aMCI (AD-aMCI).

To explore this lack of alignment change, the connectivity matrices of the HC group are adapted by replacing the functional connectivity of one ROI. Specifically, the posterior cingulate gyrus (pCG) was selected as a prominent region in the DMN where we would have expected to see change due to AD. The pCG was taken from nine AD subjects and substituted into nine of the HC subjects. By comparing these altered HC connectivity matrices with those of the original HC group, more alignment shifts are seen than in the AD-HC comparison. For the subjects with a substituted pCG, there are now 16 significant changes in eigenvector alignment, whereas in the AD versus HC comparison there were only 2 significant changes in alignment (despite the weighting of functional connectivities to and from the pCG being the same for both the altered HC and AD groups). Unsurprisingly, no other ROI in this comparison has more than 1 significant alignment change. The most significantly affected ROIs from the addition of the AD subject's pCG connectivity, in terms of eigenvector alignment, are the right amygdala ($p = 0.003$), right occipital fusiform gyrus ($p = 0.006$), left posterior temporal fusiform cortex ($p = 0.009$), left pallidum ($p = 0.013$), left cuneus ($p = 0.013$) and right lingual gyrus ($p = 0.015$).

It is possible that connectivity variations between each subject contributed to the higher number of significant alignment changes, when substituting the pCG from AD subjects into HC subjects. However, by performing the same substitution process with the left Heschl's gyrus (which experiences 26 significant alignment changes between AD and HC) 22 significant alignment changes are seen with 15 of those the same as in the AD-HC comparison.

Interestingly, this ROI substitution can not be detected as easily when only considering EC. There is a decrease in the mean EC value for the pCG ROI, but this is not significant when comparing the alterated HC connectivity matrices with HC subjects nor does it produce a significant difference when comparing with other ROI

individually.

Finally, applying the substitution approach for the anterior cingulate gyrus only increases the number of significant alignment changes from 0 to 3. Therefore, in the following section another aspect is considered for why these DMN ROI do not present with many significant alignment changes.

Functional Connectivity

The number of significant changes in functional connectivity are investigated to highlight one reason for why there is a difference between these results and that of eigenvector alignment. For AD versus HC, the greatest number of changes in functional connectivity with respect to other ROIs were seen for the left paracingulate gyrus, right Planum Polare and right pallidum with 15 significant changes each. The left paracingulate gyrus and right planum polare are highlighted by eigenvector alignment in the Alzheimer's Disease section, but the right pallidum is a notable omission. This appears to be partly due to its lack of consistently high or low alignments to any ROIs, especially in HC subjects where the standard deviation of all the mean alignments for the right pallidum is $\sigma = 0.185$. This compares with the alignments of the left paracingulate gyrus ($\sigma = 0.295$) and right planum polare ($\sigma = 0.309$).

Another ROI with a relatively high number of significant functional connectivity changes and a lack of consistently high or low alignments to any ROI, in either HC or AD subjects, is the anterior cingulate gyrus ($\sigma = 0.184$ for HC group). This ROI is noted in the previous section for not experiencing many significant alignment changes, but it does show 11 significant changes in functional connectivity.

Discussion

The results from applying CST with the communities of dynamical influence [12] supports the reasoning that AD subjects would be expected to show the greatest change in functional connectivity and that the contrast would be most obvious when compared with the HC group. From comparing a set of constant thresholds lower thresholds were found to create greater differences in the sizes of least influential communities, which are more likely to be impacted by the removal of low weighted connections. Meanwhile greater differences in the most influential communities were seen when applying higher constant thresholds.

The insights gained from eigenvector alignment are not exclusive to using three dominant eigenvectors. The Introduction section notes that a range of eigenvectors have been employed previously to identify neuronal circuitry. The use of the most dominant eigenvectors simply ensures that the changes exposed are amongst the most important in terms of information flow around the brain, as captured by functional connectivity. The use of three eigenvectors is supported in [12] for identifying influential leaders in systems governed by consensus dynamics. Our findings appear to support the use of three eigenvectors, with AD subjects most clearly identified from the size of their most and least influential communities of dynamical influence (CDI) when using three dominant eigenvectors and applying the Cluster-Span Threshold.

In Figure 3, we report on a restructuring of the AD subjects' brains in response to disruption of the commissural system [29]. Either side of posterior superior temporal gyrus (pSTG) becomes increasingly separated, in terms of alignment, as a person progresses from HC $\rightarrow$ aMCI $\rightarrow$ AD. We show that this separation results in a very significant increase in alignment to the Brainstem ROI for both sides of the pSTG. This result has a high significance due to the consistent separation of the Brainstem with the bilateral pSTG in HC subjects. This highlights compensatory restructuring of the

brain's connections in AD, especially for the right pSTG where the Brainstem transitions from being one of the least aligned ROIs in HC subjects to one of the most aligned in AD subjects.

It is acknowledged that ROIs not strongly associated with the AD pathology experience a large number of significant alignment changes – such as the Heschl's gyrus, planum polare, and planum temporale – whilst other regions that are known to lose functional connectivity maintain a similar alignment to that seen in Healthy Control subjects – such as the ROIs in the Default Mode Network (DMN).

The finding of significant disruption to left Heschl's gyrus (also referred to as the transverse temporal gyrus) in AD subjects is interesting. The volume of left Heschl's gyrus has been highlighted as having the potential to discriminate people with AD from healthy controls (sensitivity 86.5%; specificity 79.7%) [34]. In [35], the right auditory cortex is proposed to be initially more resistant to degenerative changes than the left auditory cortex. This conclusion was drawn from the finding that ipsilateral auditory processing is delayed only in the left side for AD subjects. Given the findings in [35], it is worth noting that the biggest increase in alignment when comparing the AD and aMCI group is between the right Heschl's gyrus and the right posterior inferior temporal gyrus. This auditory asymmetry has also been noted in [36] where significant differences in connectivity between the left auditory cortex and the posterior hippocampus is found in carriers of the APOEϵ4 protein, which represents a high risk of AD diagnosis. Our findings contribute to accumulating evidence that during the course of AD, Heschl's gyrus appears to be undergoing substantial changes in volume, connectivity and influence.

It is well-established that the DMN experiences reduced functional connectivity in those with AD [33, 37, 38], therefore changes in eigenvector centrality (EC) and alignment may be anticipated. Differences in EC are seen for the DMN including a clear decrease in EC for the anterior cingulate gyrus (aCG) in AD with respect to both HC and aMCI groups. But the same was not seen for eigenvector alignment, with two reasons highlighted for this. Firstly, eigenvector alignment assesses relative changes in the connectivity network. Replacing the posterior cingulate gyrus (pCG) of HC subjects, with that of AD subjects, demonstrates that in isolation significant changes in this ROI's functional connectivity would result in significant shifts in eigenvector alignment. Another contributing factor is a lack of consistently high or low alignments to any ROI, as is the case for the aCG in each of the groups. This lack of consistency ensures that only a few significant alignment shifts are detected.

When substituting the pCG from AD subjects into connectivity matrices of healthy controls, the most significant change in alignment is with the right amygdala. This finding supports the importance of the amygdala as an indicator of AD [39], especially when considered alongside the finding that the biggest decrease in alignment from aMCI to AD is between the right amygdala and right frontal orbital cortex, and that in AD the right hippocampus is most closely aligned with the left amygdala. In [39] the atrophy of the amygdala, combined with encoding-induced abnormal alpha desynchronized activity over the posterior cingulate gyrus, produced the best accuracy for predicting AD conversion from aMCI.

This set of analyses has shown that eigenvector alignment can offer insights into the network properties of the brain, and may be usefully applied in conjunction with other methods to gain a fuller picture of the brain's function. Even within eigenvector alignment, there are a number of elements that can be combined or explored separately. For example, the number of significant alignment changes for a ROI may be few, but these changes might be large in magnitude and extremely important for brain function (e.g., a cognitive ability could be impaired through a disconnection between two single ROIs). For that reason, in future studies, as was done here, it may be important to

consider both the number of changes in alignment and also the magnitude of the changes between that ROI and other ROIs. There are challenges in how to best summarise the findings from eigenvector alignment both within groups and when performing group comparisons. Simple visualisation of results summaries, for example, are difficult given that alignment is assessed between every combination of ROIs. The number of alignment changes for each ROI could be back-projected onto a standard brain template, but how to best visualise or convey the rich insights from eigenvector alignment remains an open question.

Conclusions

Eigenvector alignment is demonstrated to detect significant structural changes in functional connectivity networks of AD and aMCI subjects by comparing the alignment of ROI position vectors in a Euclidean space defined by the system's dominant eigenvectors. Eigenvector connectivity (EC) results were often distinct from those of eigenvector alignment. The ROIs in the Default Mode Network (DMN) highlighted that significant changes in functional connectivity and EC, in AD, do not guarantee significant changes in alignment. For the DMN this lack of alignment change is thought to have two components. Firstly, eigenvector alignment reflects relative changes in network structure and therefore widespread connectivity changes, in AD, can mask the significant losses in connectivity among central DMN ROIs. These widespread changes across the brain regions that comprise the DMN, result in the DMN ROIs maintaining relative alignment and, hence, a similar network structure in AD and HC subjects. Secondly, prominent DMN regions, such as the anterior cingulate gyrus (aCG), display significant changes in functional connectivity and EC but only a few significant eigenvector alignment changes. This is shown to be, in part, due to a lack of consistently high or low alignments to other ROI in AD and HC subjects. Without either a clear alignment or lack of alignment to any other ROI, functional connectivity changes do not convert into significant changes in eigenvector alignment.

Prominent decreases in eigenvector alignment were found between the left and right sides of the posterior superior temporal gyrus (pSTG) and the superior parietal lobules. In the case of pSTG, this coincided with a very significant bilateral increase in alignment with the brainstem. For the parahippocampal gyrus (PHG), our results aligned with the known pathology of AD whereby the posterior PHG was seen to experience a large number of significant alignment changes in aMCI subjects while the anterior region displayed far more alignment changes in AD subjects. The left Heschl's gyrus and bilateral planum polare are some of the ROIs that experience the largest number of alignment changes when comparing the AD and HC subjects. Bilaterally, these two regions are well-aligned with each other in HC subjects, but this alignment is significantly reduced in AD. In aMCI, a number of the most significantly affected ROIs are noted for significant and consistent realignment with the Heschl's gyrus and planum polare.

This analysis formed a proof of concept for eigenvector alignment, which has demonstrated its potential for wider application in large studies that can identify reliable biomarkers of disease.

References

1. Gili T, Cercignani M, Serra L, Perri R, Giove F, Maraviglia B, et al. Regional brain atrophy and functional disconnection across Alzheimer's disease evolution. Journal of Neurology, Neurosurgery & Psychiatry. 2011;82(1):58–66.

2. Greicius MD, Krasnow B, Reiss AL, Menon V. Functional connectivity in the resting brain: a network analysis of the default mode hypothesis. Proceedings of the National Academy of Sciences. 2003;100(1):253–258.

3. Rubinov M, Sporns O. Complex network measures of brain connectivity: uses and interpretations. Neuroimage. 2010;52(3):1059–1069.

4. Karwowski W, Vasheghani Farahani F, Lighthall N. Application of graph theory for identifying connectivity patterns in human brain networks: a systematic review. frontiers in Neuroscience. 2019;13:585. doi:10.3389/fnins.2019.00585.

5. Fornito A, Zalesky A, Breakspear M. Graph analysis of the human connectome: promise, progress, and pitfalls. Neuroimage. 2013;80:426–444.

6. Tijms BM, Wink AM, de Haan W, van der Flier WM, Stam CJ, Scheltens P, et al. Alzheimer's disease: connecting findings from graph theoretical studies of brain networks. Neurobiology of aging. 2013;34(8):2023–2036.

7. de Vico Fallani F, Richiardi J, Chavez M, Achard S. Graph analysis of functional brain networks: practical issues in translational neuroscience. Philosophical Transactions of the Royal Society B: Biological Sciences. 2014;369(1653):20130521.

8. Smith K, Azami H, Parra MA, Starr JM, Escudero J. Cluster-span threshold: An unbiased threshold for binarising weighted complete networks in functional connectivity analysis. In: 2015 37th Annual International Conference of the IEEE Engineering in Medicine and Biology Society (EMBC). IEEE; 2015. p. 2840–2843.

9. Dawe B, Procter A, Philpot M. Concepts of mild memory impairment in the elderly and their relationship to dementia—a review. International Journal of Geriatric Psychiatry. 1992;7(7):473–479.

10. Apostolova LG, Dutton RA, Dinov ID, Hayashi KM, Toga AW, Cummings JL, et al. Conversion of mild cognitive impairment to Alzheimer disease predicted by hippocampal atrophy maps. Archives of neurology. 2006;63(5):693–699.

11. Badhwar A, Tam A, Dansereau C, Orban P, Hoffstaedter F, Bellec P. Resting-state network dysfunction in Alzheimer's disease: a systematic review and meta-analysis. Alzheimer's & Dementia: Diagnosis, Assessment & Disease Monitoring. 2017;8:73–85.

12. Clark R, Punzo G, Macdonald M. Network communities of dynamical influence. Scientific reports. 2019;9(1):1–13. doi:10.1038/s41598-019-53942-4.

13. Newman ME. Modularity and community structure in networks. Proceedings of the national academy of sciences. 2006;103(23):8577–8582.

14. Clark R, Nikolova N, Macdonald M, McGeown WJ. Network influence based classification and comparison of neurological conditions. In: International Conference on Complex Networks and Their Applications. Springer; 2019. p. 842–853.

15. Lohmann G, Margulies DS, Horstmann A, Pleger B, Lepsien J, Goldhahn D, et al. Eigenvector centrality mapping for analyzing connectivity patterns in fMRI data of the human brain. PloS one. 2010;5(4).

16. Zuo XN, Ehmke R, Mennes M, Imperati D, Castellanos FX, Sporns O, et al. Network centrality in the human functional connectome. Cerebral cortex. 2012;22(8):1862–1875.

17. Friston K, Frith CD, Fletcher P, Liddle P, Frackowiak R. Functional topography: multidimensional scaling and functional connectivity in the brain. Cerebral cortex. 1996;6(2):156–164.

18. Friston KJ. Functional and effective connectivity: a review. Brain connectivity. 2011;1(1):13–36.

19. Varshney LR, Chen BL, Paniagua E, Hall DH, Chklovskii DB. Structural properties of the Caenorhabditis elegans neuronal network. PLoS computational biology. 2011;7(2).

20. Clark RA, Macdonald M. Eigenvector-based community detection for identifying information hubs in neuronal networks. BioRxiv. 2018; p. 457143.

21. Mascali D, DiNuzzo M, Gili T, Moraschi M, Fratini M, Maraviglia B, et al.. Resting-state fMRI in dementia patients; 2015. Harvard Dataverse. Available from: `http://doi.org/10.7910/DVN/29352`.

22. McKhann G, Drachman D, Folstein M, Katzman R, Price D, Stadlan EM. Clinical diagnosis of Alzheimer's disease: Report of the NINCDS-ADRDA Work Group* under the auspices of Department of Health and Human Services Task Force on Alzheimer's Disease. Neurology. 1984;34(7):939–939. doi:10.1212/wnl.34.7.939.

23. Petersen RC, Doody R, Kurz A, Mohs RC, Morris JC, Rabins PV, et al. Current concepts in mild cognitive impairment. Archives of neurology. 2001;58(12):1985–1992. doi:10.1001/archneur.58.12.1985.

24. Whitfield-Gabrieli S, Nieto-Castanon A. Conn: a functional connectivity toolbox for correlated and anticorrelated brain networks. Brain connectivity. 2012;2(3):125–141. doi:10.1089/brain.2012.0073.

25. Ashburner J, Friston K. Unified segmentation. NeuroImage;26.

26. Alakörkkö T, Saarimäki H, Glerean E, Saramäki J, Korhonen O. Effects of spatial smoothing on functional brain networks. European Journal of Neuroscience. 2017;46(9):2471–2480. doi:10.1111/ejn.13717.

27. Behzadi Y, Restom K, Liau J, Liu TT. A component based noise correction method (CompCor) for BOLD and perfusion based fMRI. Neuroimage. 2007;37(1):90–101. doi:10.1016/j.neuroimage.2007.04.042.

28. Smith K, Abasolo D, Escudero J. A comparison of the cluster-span threshold and the union of shortest paths as objective thresholds of EEG functional connectivity networks from Beta activity in Alzheimer's disease. In: 2016 38th Annual International Conference of the IEEE Engineering in Medicine and Biology Society (EMBC). IEEE; 2016. p. 2826–2829.

29. Thompson P, Moussai J, Zohoori S, Goldkorn A, Khan A, Mega M, et al. Cortical variability and asymmetry in normal aging and Alzheimer's disease. Cerebral Cortex (New York, NY: 1991). 1998;8(6):492–509.

30. Burgmans S, van Boxtel M, van den Berg K, Gronenschild E, Jacobs H, Jolles J, et al. The posterior parahippocampal gyrus is preferentially affected in age-related memory decline. Neurobiology of aging. 2011;32(9):1572–1578.

31. Echávarri C, Aalten P, Uylings HB, Jacobs H, Visser PJ, Gronenschild E, et al. Atrophy in the parahippocampal gyrus as an early biomarker of Alzheimer's disease. Brain Structure and Function. 2011;215(3-4):265–271.

32. Raji CA, Lopez O, Kuller L, Carmichael O, Becker J. Age, Alzheimer disease, and brain structure. Neurology. 2009;73(22):1899–1905.

33. Agosta F, Pievani M, Geroldi C, Copetti M, Frisoni GB, Filippi M. Resting state fMRI in Alzheimer's disease: beyond the default mode network. Neurobiology of aging. 2012;33(8):1564–1578.

34. Hänggi J, Streffer J, Jäncke L, Hock C. Volumes of lateral temporal and parietal structures distinguish between healthy aging, mild cognitive impairment, and Alzheimer's disease. Journal of Alzheimer's Disease. 2011;26(4):719–734.

35. Pekkonen E, Jääskeläinen IP, Hietanen M, Huotilainen M, Näätänen R, Ilmoniemi RJ, et al. Impaired preconscious auditory processing and cognitive functions in Alzheimer's disease. Clinical Neurophysiology. 1999;110(11):1942–1947.

36. Harrison TM, Burggren AC, Small GW, Bookheimer SY. Altered memory-related functional connectivity of the anterior and posterior hippocampus in older adults at increased genetic risk for A lzheimer's disease. Human brain mapping. 2016;37(1):366–380.

37. Greicius MD, Srivastava G, Reiss AL, Menon V. Default-mode network activity distinguishes Alzheimer's disease from healthy aging: evidence from functional MRI. Proceedings of the National Academy of Sciences. 2004;101(13):4637–4642.

38. Weiler M, Teixeira CVL, Nogueira MH, de Campos BM, Damasceno BP, Cendes F, et al. Differences and the relationship in default mode network intrinsic activity and functional connectivity in mild Alzheimer's disease and amnestic mild cognitive impairment. Brain connectivity. 2014;4(8):567–574.

39. del Val LP, Cantero JL, Atienza M. Atrophy of amygdala and abnormal memory-related alpha oscillations over posterior cingulate predict conversion to Alzheimer's disease. Scientific reports. 2016;6:31859.